AGU PUBLICATIONS

Water Resources Research

RESEARCH ARTICLE
10.1002/2015WR016908

The relative stability of salmon redds and unspawned streambeds

Todd H. Buxton[1,2], John M. Buffington[3], Elowyn M. Yager[4], Marwan A. Hassan[5], and Alexander K. Fremier[6]

[1]Center for Ecohydraulics Research, University of Idaho, Boise, Idaho, USA, [2]Now at US Fish and Wildlife Service, Trinity River Restoration Program, Weaverville, California, USA, [3]Rocky Mountain Research Station, U. S. Forest Service, Boise, Idaho, USA, [4]Department of Civil Engineering, Center for Ecohydraulics Research, University of Idaho, Boise, Idaho, USA, [5]Department of Geography, University of British Columbia, Vancouver, British Columbia, Canada, [6]School of the Environment, Washington State University, Pullman, Washington, USA

Key Points:
- Spawning loosens streambeds and decrease forces required for grain movement
- Boundary shear stress is elevated on redd topography relative to planar beds
- Presence of salmon nests increases bed load transport in streams

Correspondence to:
T. H. Buxton,
todd_buxton@fws.gov

Citation:
Buxton, T. H., J. M. Buffington, E. M. Yager, M. A. Hassan, and A. K. Fremier (2015), The relative stability of salmon redds and unspawned streambeds, *Water Resour. Res.*, *51*, 6074–6092, doi:10.1002/2015WR016908.

Received 10 JAN 2015
Accepted 3 JUL 2015
Accepted article online 14 JUL 2015
Published online 3 AUG 2015

Abstract Where female salmon build nests ("redds"), streambed material is mixed, fine sediment is winnowed, and bed material is moved into a tailspill mound resembling the shape of a dune. Completed redd surfaces are coarser and better sorted than unspawned beds, which is thought to increase redd stability because larger grains are heavier and harder to move, and sorting increases friction angles for mobility. However, spawning also loosens sediment and creates topography that accelerates flow, which can increase particle mobility. We address these factors controlling the relative stability of redds and unspawned beds in flume experiments where redds were constructed with a dynamic technique that mimics the nesting behavior of female salmon. Although redds exhibited relatively coarse surfaces, measured entrainment forces indicate particle loosening by spawning lowered grain resistance to motion by 12–37% on average compared to unspawned beds. In addition, for the same discharges, boundary shear stress was 13–41% higher on a redd due to flow convergence on the tailspill. Visual measurements of particle entrainment further indicated redd instability, as bed-average shear stress was 22% lower at incipient motion and 29% lower at the discharge that mobilized all grain sizes on a redd. Overall, results demonstrate that redds are unstable compared to unspawned beds, which increases the risk of scour for buried eggs but may facilitate fine sediment flushing and improve the quality of spawning gravels for future generations of spawners. Therefore, managing salmon returns to increase streambed disturbance may be an effective tool for reducing sedimentation impacts on salmon reproduction.

1. Introduction

The decline of Pacific salmon (*Oncorhynchus* spp.) outside Alaska in the past century has been met with significant efforts to bolster populations, but few have shown much success [*Lackey*, 2000]. Although a single solution for reversing the salmon's decline is unlikely, stream habitats utilized by salmon, specifically riffles, pools, and the intergravel environment, are thought to be limiting factors due to their influence on survival of juvenile salmonids [*Nehlsen et al.*, 1991; *Greig et al.*, 2005]. Stream habitats are structured by interactions between sediment transport (e.g., bed mobility, patterns of sediment entrainment and deposition, and bank erosion), channel roughness (e.g., stream banks, large wood, and boulders), and the magnitude and size distribution of the sediment supply [*Madej*, 1999]. The act of salmon building nests ("redds") modifies stream habitats [*Gottesfeld et al.*, 2004], streambed roughness [*Montgomery et al.*, 1996], and sediment transport rates during spawning [*Hassan et al.*, 2008]. The role of salmon spawning on streambed stability and sediment transport after redds are constructed is less understood. This knowledge gap exists primarily due to difficulty in observing the onset of grain motion and scour on redds relative to unspawned beds during elevated, often turbid stream flows.

Spawning salmon build redds to protect their eggs from predation and damage from agitation and bed scour [*Smirnova*, 1955]. Redd construction proceeds by the female using rapid undulations of her tail fin to hydraulically excavate a pit in the streambed. This action flushes a portion of the fine sediment into the water column to be carried downstream and mobilizes coarser sediment a short distance into a dune-like mound called a tailspill [*Burner*, 1951]. Grains too large to be moved accumulate in the pit where the female deposits a portion of her eggs for fertilization once the pit is sufficiently deep (0.10–0.50 m depending on

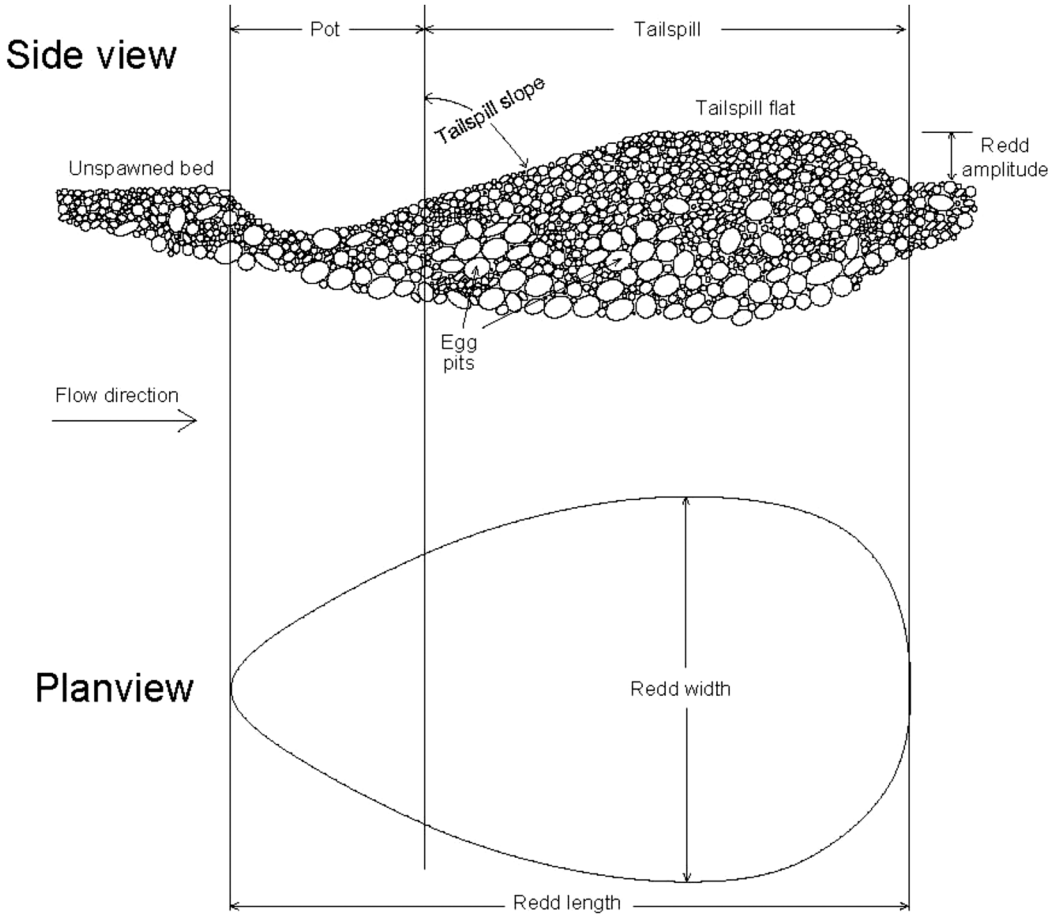

Figure 1. Side and plan view of a salmon redd (adapted from *Buxton et al.* [2015]).

fish size; *DeVries*, 1997]. The female then covers the fertilized eggs with sediment excavated from the next pit that is excavated a short distance upstream. Sequences of excavation and filling are repeated until several egg pits are built [*Burner*, 1951] and the completed redd exhibits a tailspill mound and an upstream depression called a pot (Figure 1). Redd morphology is similar between species in the genus *Oncorhynchus* [*Kondolf*, 1988], yet redd structures vary in surface area (0.6–9.4 m^2; *Bjornn and Reiser*, 1991] depending on compaction of the bed, caliber of substrate, velocity and depth of flow, slope of the channel, and body size of the female [*Kondolf and Wolman*, 1993]. However, the size of the spawning population is the primary control of bed disturbance area, since mass spawning can disrupt the entire channel bed [*Hassan et al*., 2008] compared to relatively small populations of salmon that tend to spawn in discrete patches of relatively high-quality habitat [*Isaak et al*., 2007].

Spawning in both high and low densities modifies streambeds by mixing sediment [*Gottesfeld et al*., 2004], purging fines [*DeVries*, 2012], coarsening and sorting surface grains [*Kondolf and Wolman*, 1993], and loosening grain packing [*Montgomery et al*., 1996]. These alterations benefit salmon reproduction by promoting hyporheic flow that oxygenates eggs and transports metabolic waste from egg pits [*Chapman*, 1988; *Tonina and Buffington*, 2009]. However, it is unclear whether spawning activity increases or decreases the stability of streambeds. *Montgomery et al*. [1996] predicted that critical conditions for sediment entrainment are around 2 times higher on solitary redds than unspawned beds due to spawning activity that coarsens and sorts grains. Coarsening promotes stability because larger grains are heavier and generally harder to move than smaller grains, while sorting tends to stabilize grains by increasing friction angles for grain mobility [*Buffington et al*., 1992]. Although *Montgomery et al*. [1996] recognized that bed loosening by spawning may destabilize redds to some degree, they were not able to quantify that effect. *Montgomery et al*. [1996] also calculated that form drag generated by redds in proximity to one another increased bed stability by an

additional 64%. However, calculations of redd stability have not been supported by field observations of increased scour on solitary redds [*Lisle*, 1989; *Bigelow*, 2003] and redds in high densities [*Rennie and Millar*, 2000]. This suggests the destabilizing effects of spawning, including bed loosening and elevated boundary shear stress on redd topography, are important considerations in evaluating redd stability.

Our goal is to resolve whether the stabilizing effects of spawning (grain coarsening and sorting) are offset by destabilizing factors (bed loosening and flow convergence over redds) to cause redds to be less stable than unspawned streambeds. Solving this problem is important for linking spawning disturbance to thresholds of sediment mobility, which, in part, govern the structure, quality, and availability of stream habitats that salmon use for reproduction [*Gottesfeld et al*., 2004]. To accomplish our goal, we conducted experiments in a laboratory flume using simulated redds and water worked ("unspawned") beds of mixed-grain sizes scaled from field measurements. In experiment 1, we evaluated grain stability on redds and unspawned beds using a hand-held load cell to measure the downstream force required for particle entrainment. In experiment 2, we measured flow velocity profiles using particle image velocimetry (PIV) to estimate boundary shear stresses with the log-profile method on a redd and adjacent unspawned bed. In experiment 3, we made visual measurements of sediment entrainment and measured bulk transport rates for spawned and unspawned surfaces.

2. Materials and Methods

2.1. Field Measurements

Chum salmon (*O. keta*) redd dimensions and grain-size distributions in the experiments were scaled from field measurements of these parameters in Kennedy Creek near Olympia, Washington, USA. The flume model was generic rather than specific because no other details of the creek were reproduced in the flume. The study reach in Kennedy Creek is a third-order, gravel-bed channel that exhibits a pool-riffle-run morphology, with pools forced by large wood and bedrock outcrops. The annual hydrograph is rainfall dominated, with high flows occurring November–March, and chum salmon spawning occurring September–December. Redd dimensions (length, width, and amplitude), streambed sediments, and the channel slope (0.005) were surveyed in a run in mid-December between high flows on the creek.

The size distribution of sediment in Kennedy Creek was quantified with a bulk sample (68.6 kg) collected on an unspawned portion of a dewatered lateral bar where chum salmon had spawned during a recent high flow event. The depth of the sample (0.20 m) was based on the average depth of 33 egg pockets (0.21 m) measured for chum redds in Kennedy Creek by *Peterson and Quinn* [1996]. The mass of the largest grain diameter in the sample (90.5 mm) was about 1.5% of the total sample weight, which is close to the 1% criterion suggested by *Church et al*. [1987] for requisite sample size. The size distribution by weight was determined by sieving sediment in half-phi intervals from -1 to -6.5 (2–90.5 mm) and weighing each size class to the nearest 0.1 kg.

The length, width, and amplitude of 12 recently completed redds were measured in locations surrounded by unspawned substrate and located away from obstructions (large wood, stream banks, and boulders) that can distort the common teardrop shape of redds [*Burner*, 1951]. Evidence for recent completion of measured redds included the presence of a spawned-out female guarding the nest or no indication of redd erosion by flow or fish migration. Redd lengths were measured to within ± 0.05 m with a survey rod from the upstream edge of the pot to the downstream edge of the tailspill (Figure 1). Redd widths were measured with the same accuracy at the widest portion of the structure. Redd amplitudes were measured to within ± 0.02 m with a carpenters level and survey rod from the peak height of the redd to the adjacent unspawned bed (Figure 1).

2.2. Experimental Scaling

Scaling physical dimensions and flow parameters requires similitude of Froude (*Fr*) and Reynolds numbers (*Re*) between the flume and Kennedy Creek. Reynolds numbers are given by

$$Re = \frac{\rho \bar{u} h}{\mu} \tag{1}$$

where ρ and μ are the density (kg m^{-3}) and dynamic viscosity of water (kg m s^{-1}), respectively, $\bar{u}$ is average flow velocity (m s^{-1}), and h is flow depth (m). Froude numbers are defined as

Table 1. Scaled Redd Dimensions and Median Grain Sizes (D_{50}) and Sorting Parameters (σ) for Surface Particles on Redds and Unspawned Beds (US) in Flume Experiments 1–3

	Experiment 1									Experiment 2		Experiment 3	
Sediment Mix	1			2			3			1		4	
Bed Surface	US	LT[a] Redd	RT[a] Redd	US	LT[a] Redd	RT[a] Redd	US	LT[a] Redd	RT[a] Redd	US	Redd	US	Redd
Length (m)		0.93	0.97		0.86	0.92		0.85	0.86		0.95		0.90
Width (m)		0.50	0.50		0.50	0.54		0.52	0.51		0.62		0.61
Height (m)		0.04	0.04		0.03	0.03		0.05	0.05		0.07		0.06
TS angle[b]		11	15		13	13		12	11		16		18
D_{50} (mm)	5.0	9.6	7.7	5.1	7.6	7.3	7.4	12.4	11.3	8.4	8.6	5.8	6.2
σ[c]	1.24	0.98	0.98	1.25	1.01	0.94	1.35	0.88	0.85	1.27	1.13	1.25	0.86

[a]Left (LT) and right (RT) indicates redds located to either side of the unspawned bed.
[b]Angles of the tailspill slope (TS) measured in degrees from horizontal with an electronic level.
[c]For comparison to values in *Montgomery et al.* [1996], sorting parameters calculated as the inclusive graphic standard deviation with $(\phi_{95}-\phi_{16})/4+(\phi_{95}-\phi_5)/6.6$ [*Folk*, 1974], where ϕ is in log base 2 units and subscripts indicate percentiles of the grain-size distribution. Lower values of σ indicate better sorting.

$$Fr=\frac{\bar{u}}{(gh)^{0.5}} \tag{2}$$

where g is gravitational acceleration (9.81 m s^{-2}). Because it is not possible to simultaneously scale both Fr and Re, we used Fr scaling to model redd dimensions and flow velocity and depth during redd construction that occurred in fully turbulent discharges ($Re \geq 4.2 \times 10^4$). With Fr scaling, the model is related to the prototype with a length factor (L_L)

$$\frac{L_p}{L_m}=\frac{W_p}{W_m}=\frac{\Delta_p}{\Delta_m}=\frac{D_p}{D_m}=\frac{h_p}{h_m}=L_L \tag{3}$$

where L, W, and Δ are the redd length, width, and amplitude, respectively, D is grain diameter and the p and m subscripts indicate the prototype and model, respectively. Using equation (3), redds constructed in the flume were scaled from the average length (2.7 m; standard deviation (s) = 0.9 m), width (1.6 m; s = 0.5 m), and amplitude (0.10 m; s = 0.04 m) of redds measured in Kennedy Creek with an L_L = 3 (Table 1). The grain-size distribution in Kennedy Creek was also scaled with L_L = 3, which enabled us to create sediment mixtures for the experiments that approximated the scaled grain-size distribution (mix 1–4; Figure 2).

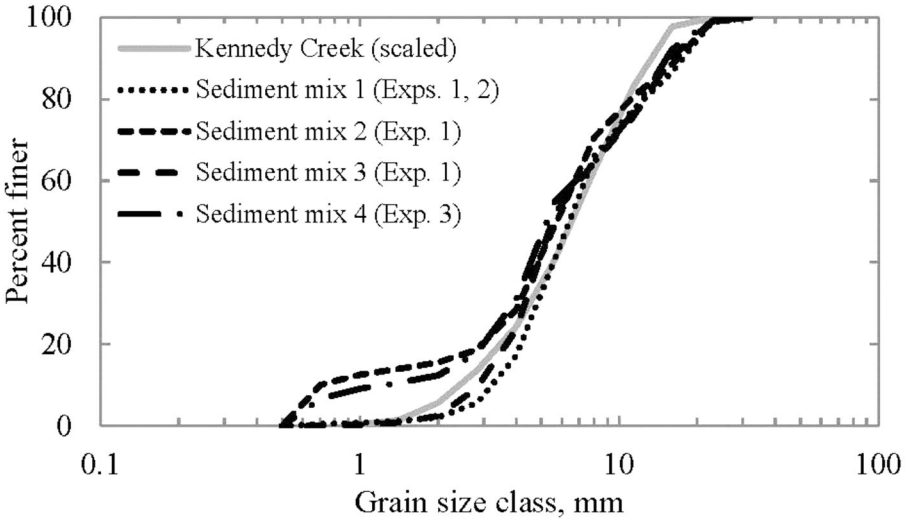

Figure 2. Cumulative grain-size distributions for bulk sediment mixtures 1–4 used in the flume experiments relative to scaled grain sizes measured in Kennedy Creek (solid grey line).

To avoid disturbing spawning salmon in Kennedy Creek, field measurements of flow depth and velocity at redds under construction were not obtained. Instead, flow depths for redd construction in the flume were scaled with equation (3) from values reported by *Smith* [1973] for spawning chum salmon in Oregon streams (average $h_p = 0.30$ m, $s = 0.41$ m, $n = 214$). Data from *Smith* [1973] were also used to scale the flow velocity for redd construction ($\bar{u}_p = 0.73$ m s^{-1}, $s = 0.65$ m s^{-1}, $n = 214$) using

$$\frac{\bar{u}_p}{\bar{u}_m} = \sqrt{L_L} \tag{4}$$

The average flow depth (0.14 m, $s = 0.07$ m, $n = 8$) and velocity (0.45 m s^{-1}, $s = 0.04$ m s^{-1}) for constructing redds in the flume (section 2.4) were within a standard deviation of scaled flow depths ($h_m = 0.10$ m, $s_m = 0.24$ m) and velocities ($\bar{u}_m = 0.42$ m s^{-1}, $s_m = 0.38$ m s^{-1}) determined from values reported by *Smith* [1973]. In addition, the average Fr_m (0.39) during redd construction was within 10% of the Fr_p (0.43) for chum spawning according to data in *Smith* [1973]. In all experiments, the flume slope was set to that of Kennedy Creek (0.005).

2.3. Experimental Layouts

Experiments were conducted in a 20 m long by 2 m wide glass-walled flume at the Center for Ecohydraulics Research at the University of Idaho in Boise. In all experiments, fixed beds were installed in the upper 12 m of the flume to generate uniform flow using sand to gravel-sized grains glued to plywood. A lumber crib supported the fixed beds 0.14 m above the flume bottom to allow sediment to be placed to this depth in the test area that extended variable distances downstream of the fixed beds. The test area for experiment 1 (grain stability) extended 1 m downstream of the fixed beds and was 2 m wide to accommodate beds constructed in three wooden boxes (1.0 m long, 0.64 m wide) installed across the flume. The middle box held an unspawned bed, and redds were constructed in boxes on both sides of the unspawned bed (Figure 3a, Table 1).

The test area for experiment 2 (boundary shear stress) extended 1.4 m downstream and was 1 m wide so that a wooden box with these dimensions was large enough to contain a redd surrounded by an unspawned bed (Figure 3b, Table 1). Fixed beds were installed on both sides of the test bed to maintain uniform flow in experiment 2. Redds and unspawned beds were constructed in boxes in experiments 1 and 2 for lifting them from the flume after completion of experiments. In both experiments, a fixed bed also was installed for 2 m downstream of the test area to generate roughness that, along with adjustments of the flume tailgate, prevented flow from accelerating from the test areas.

For experiment 3 (grain mobility), the test area was enlarged to 2 m in the downstream direction by 2 m wide for capturing bed load from a redd and unspawned bed in three traps equally spaced across the flume at a location 1 m downstream of the test area (Figure 3c, Table 1). A plywood bed was installed for 2 m downstream of the test area to provide a platform for fastening bed load traps and to facilitate transport of mobile sediment into the traps after particles moved from the test area.

2.4. Bed Construction

Redds and unspawned beds were constructed by placing a grain mixture in the test area, screeding it flat with a shovel, and slowly wetting the sediment to expel air and settle the bed. Flow was then increased to water work the beds for a 2 h duration that began when five or more grains moved a distance of at least their diameter downstream. Water working then proceeded by increasing flow in increments to maintain a low sediment transport intensity that winnowed fine sediment, oriented grains to flow, and formed and destroyed pebble clusters [*Hassan and Church*, 2000]. Sediment was not fed into the flume during the experiments. After water working, flow was adjusted to generate scaled flow depths and velocities for constructing redds (section 2.2). To verify flow settings, spawning depths were measured to within $\pm$0.8 cm with a wading rod at the center of locations where redds were to be constructed. Flow velocities were measured to within $\pm$2% (manufacturer's specification) at six-tenths flow depth for 60 s with a pygmy flow meter at these same locations. Redds were constructed in the scaled flows with a metal spatula that was a scaled model of chum caudal fins (Appendix A). The metal spatula was operated to mimic the spawning activity of female salmonids, whereby successive episodes of pit excavation and filling were accomplished by rapid undulations of the spatula, which flushed fine grains from larger sediment, loosened grain packing, and moved sediment into the redd tailspill structure. Completed redds exhibited teardrop shapes that were

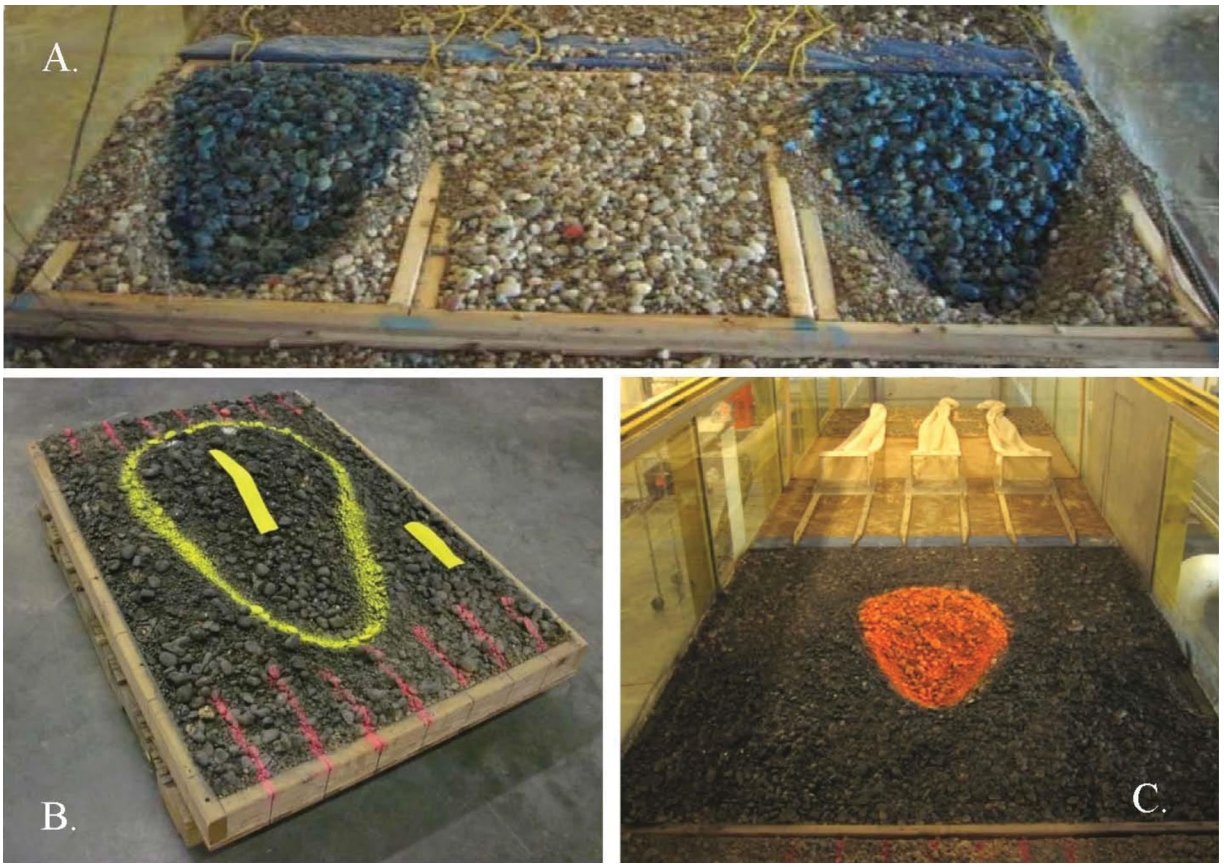

Figure 3. Redds and unspawned beds used for (a) total resistance measurements (sediment mix 1 shown), (b) flow velocity measurements with particle image velocimetry (PIV), and (c) visual measurements of grain mobility and bed load capture. Bed load traps are shown in the background of Figure 3c. The bed in Figure 3b is shown after removal from the flume, with the outline of the redd and location of PIV transects in yellow (transect on the right is for the unspawned bed). The unspawned bed in Figure 3a is shown before it was painted to distinguish surface grains from subsurface particles. Dimensions of redds in each figure are reported in Table 1.

oriented with their long axis parallel to flow (Figure 3). As in nature, the longitudinal profile of redds exhibited a pot depression and tailspill mound with an upstream sloping surface and a flat area (Figure 1).

2.5. Evaluation of Simulated Spawning

The accuracy of modeled redds was assessed by comparing their dimensions to those for chum salmon redds in three, low-gradient gravel-bed rivers: Kennedy Creek, Herman Creek near Haines, Alaska, and Lilliwaup Creek near Lilliwaup, Washington. Herman and Lilliwaup Creeks were added to increase sample size for the comparisons. Redd dimensions were measured as described in section 2.1, except to a higher degree of precision in the flume ($\pm$0.02 m) than in the field ($\pm$0.05 m). Comparisons demonstrate that dimensions and aspect ratios (Δ/L) of simulated redds were in the range of those measured for chum salmon redds in the field (scaled with $L_L = 3$, Figure 4).

Changes in median grain size (D_{50}) and sorting (σ) [*Folk*, 1974] from simulated spawning were also compared to field values measured by *Montgomery et al*. [1996] in Kennedy Creek. In experiments 1 and 2, grain-size distributions were measured with *Wolman* [1954] samples of 150 grains on redds and 220 grains on unspawned beds by lowering a small pointed stick while looking away and then measuring the apparent intermediate grain diameter to 0.1 mm with digital calipers. Diameters were apparent because particles were often partially buried and the bed surfaces were glued in place for removal from the flume, which precluded extraction of particles for measurement. In experiment 3, *Wolman* [1954] samples of 100 grains were photographically measured with Sedimetrics software [*Graham et al*., 2005a, 2005b] to avoid disturbing the beds prior to the mobility test. We used Sedimetrics because it accurately duplicates manual methods for measuring grain-size distributions, including *Wolman* [1954] pebble counts and sieving [*Graham et al*., 2005a]. We confirmed the accuracy in 18 tests with sediment mixtures used in the flume experiments,

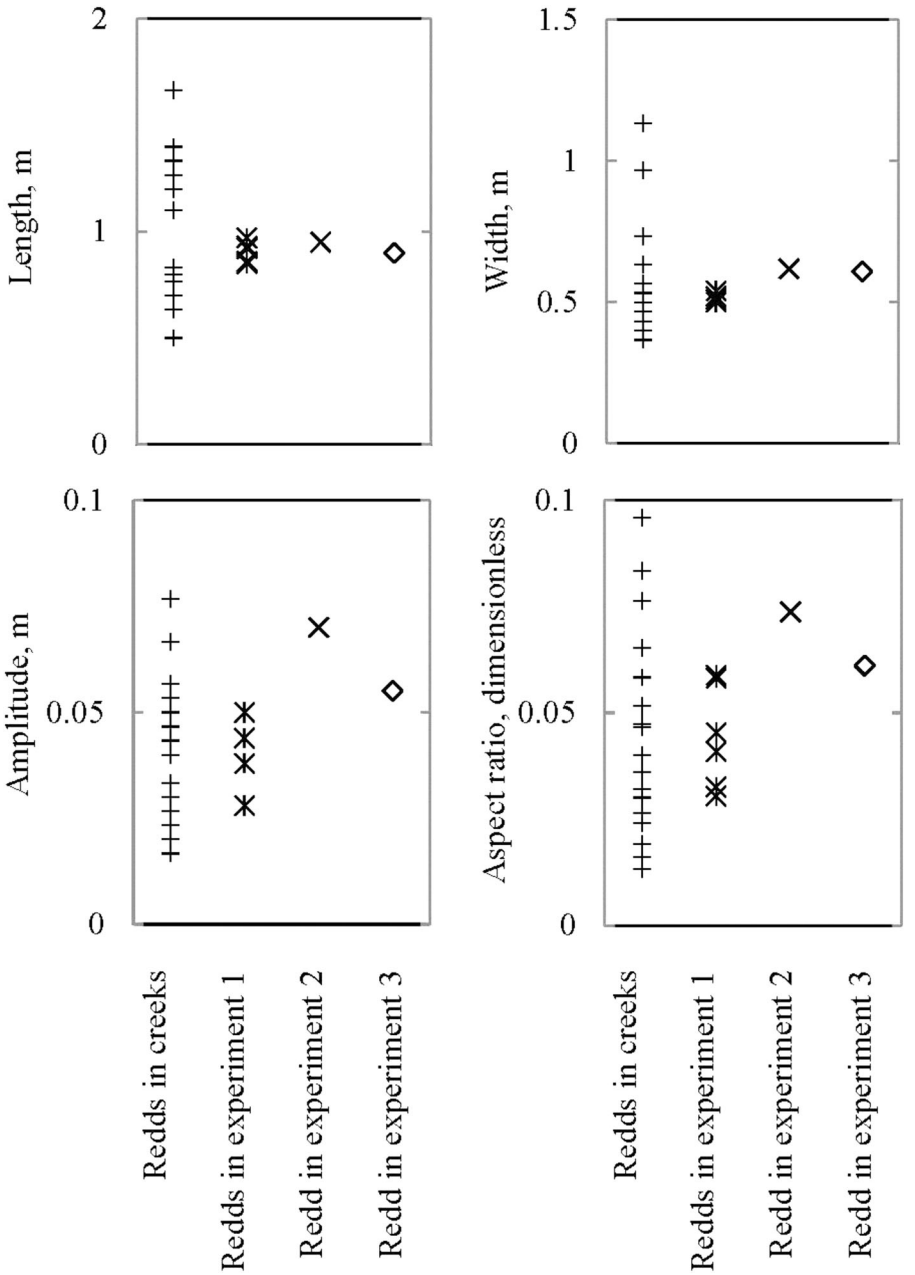

Figure 4. Redd dimensions and aspect ratios in experiments 1–3 in the flume compared to scaled values for chum salmon redds in Kennedy, Herman, and Lilliwaup Creeks. Aspect ratios are redd amplitude divided by redd length.

where photographic measurements of grain area-by-number were converted to volume-by-weight [*Kellerhals and Bray*, 1971] and compared to sieve analysis of the photographed sample. Pair-wise comparisons of grain-size distributions in each test were statistically insignificant according to *Kolmogorov-Smirnof* (*KS*) tests ($\alpha = 0.05$). Findings indicate that simulated redds had median grain sizes ($D_{50} = 8.8$ mm) that were 28% coarser on average than unspawned beds (6.3 mm; Table 1), which is close to the average percent increase reported by *Montgomery et al.* [1996] for Kennedy Creek (36%). Moreover, the average increase in grain sorting (+36%) on simulated redds ($\sigma = 0.94$) compared to unspawned beds ($\sigma = 1.28$; Table 1) was nearly identical to that measured by *Montgomery et al.* [1996] (+35%).

2.6. Experiment 1: Grain Stability

Grain stability on redds and unspawned beds was quantified with hand measurements of the total downstream force required for particle entrainment (F_{total}) in the flat and upstream sloping area of the pot, the

tailspill slope, and the tailspill flat (Figure 1). Before starting the measurements, bed surfaces were misted with spray paint to delineate undisturbed surface grains from disturbed surface grains and subsurface particles. Values of F_{total} were then measured with a FUTEK LSB210 load cell connected to a laptop computer with a FUTEK USB210 that detected the peak applied force at 10 Hz with a nominal accuracy of 0.001% (manufacturer's specification). A 3 mm diameter by 1 cm long post was inserted in the load cell for applying a push force in a downstream and bed-parallel direction on each measured grain. We pushed at the midpoint of the exposed frontal area of all grains that protruded at least partially above the local bed surface and were surrounded by undisturbed sediment [*Johnston et al.*, 1998]. With the slope of the flume set to zero, an applied force was used to push each grain a distance approximately equal to its diameter, which defined grain movement in our study. Distances of grain movement were approximate because diameters could not be measured a priori without disturbing the grain. Measurements of F_{total} were limited to the right or left half (randomly chosen by coin flip) of each bed to preserve the undisturbed half for gluing and removal from the flume for measuring grain-size distributions (section 2.5).

Resistance measurements proceeded by mobilizing a grain with the load cell, recording the type of movement (sliding, pivoting/rolling, or tilling), extracting the grain for weighing to the nearest 0.1 g, and measuring its three major axes with digital calipers to the nearest 0.1 mm. We excluded tilling motions (movement that plows neighboring grains) because grains in natural channels commonly move in a sliding or pivot/rolling motion, or a combination of the two [*Francis*, 1973]. The availability of different-sized particles limited measurements to grain-size classes from -2 to -5 phi (4–32 mm). Measurements were made for sediment mixtures 1–3, with values pooled for the two redds in a given mixture. Pooled values of F_{total} for redds and unspawned beds (in parenthesis) composed of sediment mix 1–3 were 426 (268), 416 (268), and 412 (271).

Paired measurements of F_{total} and particle weight were used to compute dimensionless friction coefficients (μ) for grains on the redds and unspawned beds. Values of μ were computed by dividing measurements of F_{total} by the weight of each measured grain (F_n), which for level, dewatered surfaces is the grain mass (m) times gravitational acceleration (g). For grains on the upstream sloping portion of the redd pot and tailspill (Figure 1), adjustments to F_{total} and F_n were necessary since a component of the grain's weight ($mg \sin \phi_{ts}$, where ϕ_{ts} is the slope of the tailspill from horizontal (Table 1)) acts downslope against F_{total} and only a portion of the grain's weight ($mg \cos \phi_{ts}$) acts perpendicular to the sloping bed surface. As such, friction coefficients for grains on sloping portions of the redd were computed as

$$\mu = \frac{F_{total} - mg \sin\phi_{ts}}{mg \cos\phi_{ts}} \tag{5}$$

2.7. Experiment 2: Boundary Shear Stress

Point estimates of boundary shear stress (τ_b) were made in streamwise transects on a solitary redd and the unspawned bed adjacent to the redd (Figure 3b) using flow velocity fields measured with two-dimensional (2-D, streamwise and vertical directions) PIV. Measurements were conducted at discharges of 0.32 and 0.64 $m^3\ s^{-1}$ that were gauged to $\pm$0.5% with an electromagnetic flow meter in the water supply to the flume. The discharge of 0.64 $m^3\ s^{-1}$ was used because it was the maximum flow rate at which we could safely enter the flume and position the beds for measuring flow velocities. The discharge of 0.32 $m^3\ s^{-1}$ was used because it was half of 0.64 $m^3\ s^{-1}$ and close to the discharge (0.25 $m^3\ s^{-1}$) at which grain incipient grain motion was visually measured on the redd (experiment 3). At discharges of 0.32 and 0.64 $m^3\ s^{-1}$, average flow depths were 11.0 and 20.1 cm on the redd and 17.5 and 26.6 cm on the unspawned bed, respectively. The length (L) and amplitude of the redd (Δ) were 90 and 6.5 cm, respectively, which made the redd's $\Delta/L = 0.07$. The relative submergence (h/Δ) of the redd was 1.7 at 0.32 $m^3\ s^{-1}$ and 3.1 at 0.64 $m^3\ s^{-1}$. Bed surfaces were glued to prevent grain movement during velocity measurements. Glue fixed grains without pooling and modifying surface roughness on the beds.

Streamwise transects for velocity measurements were 35.3 cm and 21.1 cm long on the redd and unspawned bed, respectively (Figure 3b). The transect was longer on the redd to enable velocity measurements on the flat and sloping portions of the tailspill. Velocities were not measured in the pot because the PIV laser sheet was blocked from the depression by projection of the tailspill. We believe this omission did not influence study results because recirculating flow in the pot depression [*Burner*, 1951] is unlikely to notably affect stability of the tailspill. Velocity measurements were located on the unspawned bed adjacent

to the redd and may have been influenced by flow accelerating around the redd, which could increase shear stress relative to what would occur in the absence of the redd.

Particle image velocimetry involved illuminating neutrally buoyant particles in the flow column with a dual pulse 1064 nm laser sheet oriented along the transects (Figure 3b). A high-speed camera captured images of the particles (through the glass sidewall of the flume) at 9 Hz for 120 s at vertical positions from the bed to a height of 12.3 cm. Vertical profiles were composed of 73 interrogation regions, each with an area of 0.22 cm^2. Instantaneous downstream velocities were calculated in each interrogation region using a cross-correlation analysis of the distance that particles traveled between successive images [e.g., *Adrian*, 2005]. Instantaneous velocities were averaged to give mean velocity for each interrogation region. To reduce computations, only every other vertical profile was used to estimate τ_b, which increased the streamwise distance between profiles to 0.43 cm. The number of τ_b estimates on the redd and unspawned bed was 83 and 53, respectively.

Flow velocities in the near-bed region exhibited logarithmic relations with height above the bed ($R^2 \geq 0.81$ and ≥ 0.77 on the redd and unspawned bed, respectively; Figure 6). This enabled τ_b to be estimated with the law of the wall [*Keulegan*, 1938]

$$u = \frac{u_*}{\kappa} ln\left(\frac{z}{z_o}\right) \tag{6}$$

where u is flow velocity, u_* is shear velocity ($=\sqrt{\tau_b/\rho}$), κ is von Kármán's [1930] constant (0.407), z is height above the bed, and z_0 is the roughness length scale where flow velocity is zero. We used the five lowest velocities in the logarithmic profiles (4.3–13 mm above the bed, Figure 6) to determine the slope (m) of a least squares regression between (u, ln(z)) for each profile. From the derivative $\partial(\ln(z))/\partial u$ of equation (6), $m=\kappa/u_*$, which after rearrangement enabled bed shear stress to be calculated as [*Middleton and Southard*, 1984]

$$\tau_b = \rho\left(\frac{\kappa}{m}\right)^2 \tag{7}$$

2.8. Experiment 3: Grain Mobility

Grain mobility was visually measured on a solitary redd and a nearby, unspawned bed to determine the relative stability of each surface, while mobile particles were captured in bed load traps to determine mass transport rates of surface grains. For these measurements, the redd and unspawned bed surfaces were spray-painted orange and black, respectively, to aide observations of mobility and determine the origin of surface grains captured in the traps (Figure 3c). Bed load traps had 0.3 m wide by 0.2 m tall openings and were equipped with 5 m long nets with 3.125 mm mesh openings that retained the coarsest 89% of the sediment mixtures. Visual measurements of entrainment were made and bed load traps were operated at 14 successive discharges (0.12–1.05 $m^3\ s^{-1}$), each lasting 20 min. The lowest discharge (0.12 $m^3\ s^{-1}$) was based on observations of incipient motion on redds in a preliminary experiment with a test bed composed of similar grain sizes. The peak discharge (1.05 $m^3\ s^{-1}$) was that which completed erosion of the redd to a level flush with the unspawned bed. The duration of measurements was set by the time required to adjust the flume tailgate to maintain uniform flow, when necessary, and to make and record visual measurements of grain mobility. Sediment was not supplied to the upstream end of the flume during the experiments. Bed load traps were emptied between discharges and captured sediment was dried and separated by color. Painted grains were weighed to the nearest gram to determine mass transport rates of surface grains per unit area of the redd (0.42 m^2) and unspawned bed (3.58 m^2) for each discharge. Analysis did not include subsurface grains because they were unpainted, which precluded determining their location of origin as either from the redd or unspawned portion of the bed.

Visual measurements of entrainment were made for grain diameters in size bins defined as >24 mm, 16 to <24 mm, 8 to <16 mm, 4 to <8 mm, and <4 mm. Size bins differed from half-phi gradations because it was difficult to visually measure grain diameters in such increments. We did not quantify uncertainty in our grain-size estimates, which are a source of bias in visual measurements of entrainment [*Buffington and Montgomery*, 1997]. Entrainment was defined in the visual measurements as when five or more grains in a bin moved a distance equal to their diameter in 30 s. An exception applied to grains <4 mm, which were required to evacuate their resting pocket to be classified as mobile, since movement of a lesser distance

was difficult to detect. Observations of mobility and mass transport rates were plotted against bed-averaged shear stress ($\tau_{b_{avg}}$) that was partitioned to remove wall effects (Appendix B).

3. Results

3.1. Grain Stability (Experiment 1)

Cumulative distributions of measured resistance forces (F_{total}) for grains on redd and unspawned surfaces are shown in Figure 5 for sediment mixes 1–3. Considering that redds were coarser (larger D_{50}) than unspawned beds (Table 1) and exhibited an upstream sloping tailspill surface (Figure 1), distributions of F_{total} on redds should be higher than on unspawned beds since larger grains are harder to move, especially up a sloping surface. Instead, distributions of F_{total} for the redds and unspawned bed were not significantly different for sediment mix 1 (*KS* test, $\alpha = 0.05$), while values of F_{total} were significantly lower on redds for mixes 2 and 3 (*KS* tests, $\alpha = 0.05$; Figure 5). Similar results were obtained for cumulative distributions of friction coefficients (μ, Figure 5), where average values were 12–37% lower for redds than unspawned beds. These results are consistent with *Montgomery et al.*'s [1996] observation that spawning activity loosens the bed and lowers intergranular friction, making redds less stable despite having coarser and better sorted surfaces (Table 1).

3.2. Boundary Shear Stress (Experiment 2)

Large spatial variability in boundary shear stress was captured by the high resolution of velocity measurements on the hydraulically rough surfaces of the redd and unspawned bed (Figure 6). However, variability in τ_b was higher on the redd (standard deviation (s) = 64 and 59 Pa) than the unspawned bed (s = 21 and 41 Pa) at discharges of 0.32 and 0.64 $m^3\ s^{-1}$, respectively, because of the coarser surface and dune-like topography of the redd. Point estimates of τ_b were statistically higher on the redd (*KS* test, $\alpha = 0.05$) for the lower discharge (0.32 $m^3\ s^{-1}$) and correspondingly lower relative submergence of the redd ($h/\Delta = 1.7$). Similarly, the transect-averaged τ_b was 68% higher on the redd (96 Pa; Figure 6a) than on the unspawned bed (57 Pa; Figure 6c) at 0.32 $m^3\ s^{-1}$. At the higher discharge (0.64 $m^3\ s^{-1}$), differences in transect-averaged values of τ_b between the redd (89 Pa; Figure 6b) and unspawned bed (79 Pa; Figure 6d) decreased to 13% due to larger relative submergence of the redd ($h/\Delta = 3.1$). As a result, a *KS* test ($\alpha = 0.05$) indicated that differences in point estimates of τ_b on the two surfaces were insignificant at this flow. The observed decrease in average τ_b for higher submergence of the redd is consistent with changes in τ_b on dunes [*Stoesser et al.*, 2006] and results from the redd topography being "drowned out," which causes the structure to extract less momentum from flow.

Higher shear stress on the redd at both discharges resulted from flow convergence and acceleration that progressively increased τ_b on the stoss side of the tailspill, similar to that observed on fluvial bed forms [e.g., *Venditti*, 2007; *Motamedi et al.*, 2014]. Downstream of this area, at the break in slope between the tailspill slope and flat (near −15 cm; Figures 6a and 6c), flow separation lowered τ_b below the average at both flow rates before gradually increasing to peak values near the downstream end of the transect. We note that differences in τ_b between the redd and unspawned bed are conservative because flow acceleration around the redd likely increased boundary shear stresses on the unspawned bed compared to what would occur in the absence of redd topography. The occurrence of a higher average boundary shear stress on the redd is consistent with results from *Venditti* [2007], who reported τ_b was 22–155% higher on dunes than planar beds. This comparison is particularly relevant given the similarity in aspect ratio between our redd ($\Delta/L = 0.07$; Figure 4) and *Venditti*'s [2007] dunes (0.06).

3.3. Grain Mobility (Experiment 3)

Particle mobility results are presented for the redd and unspawned surfaces in terms of competence (largest mobile grain-size bin) and bed load transport rates, both as functions of reach-average boundary shear stress ($\tau_{b_{avg}}$; Figures 7 and 8). Incipient motion was observed on the redd at a $\tau_{b_{avg}}$ (10.4 Pa) that was 22% lower than on the unspawned bed (13.4 Pa; Figure 7). These values of $\tau_{b_{avg}}$ correspond to critical dimensionless Shields stresses ($=\tau_{b_{avg}}/(\rho_s - \rho)gD$, where ρ_s is the density of sediment and D is the median diameter in the mobile grain-size class) of 0.045 for the redd and 0.109 for the unspawned bed. Mobilization of all grain sizes on the redd occurred within a narrower range of $\tau_{b_{avg}}$ (10.4–15.3 Pa for the <4 mm to >24 mm size class) than on the unspawned bed (13.4–21.5 Pa; Figure 7). Finally, the $\tau_{b_{avg}}$ that entrained all grain-size

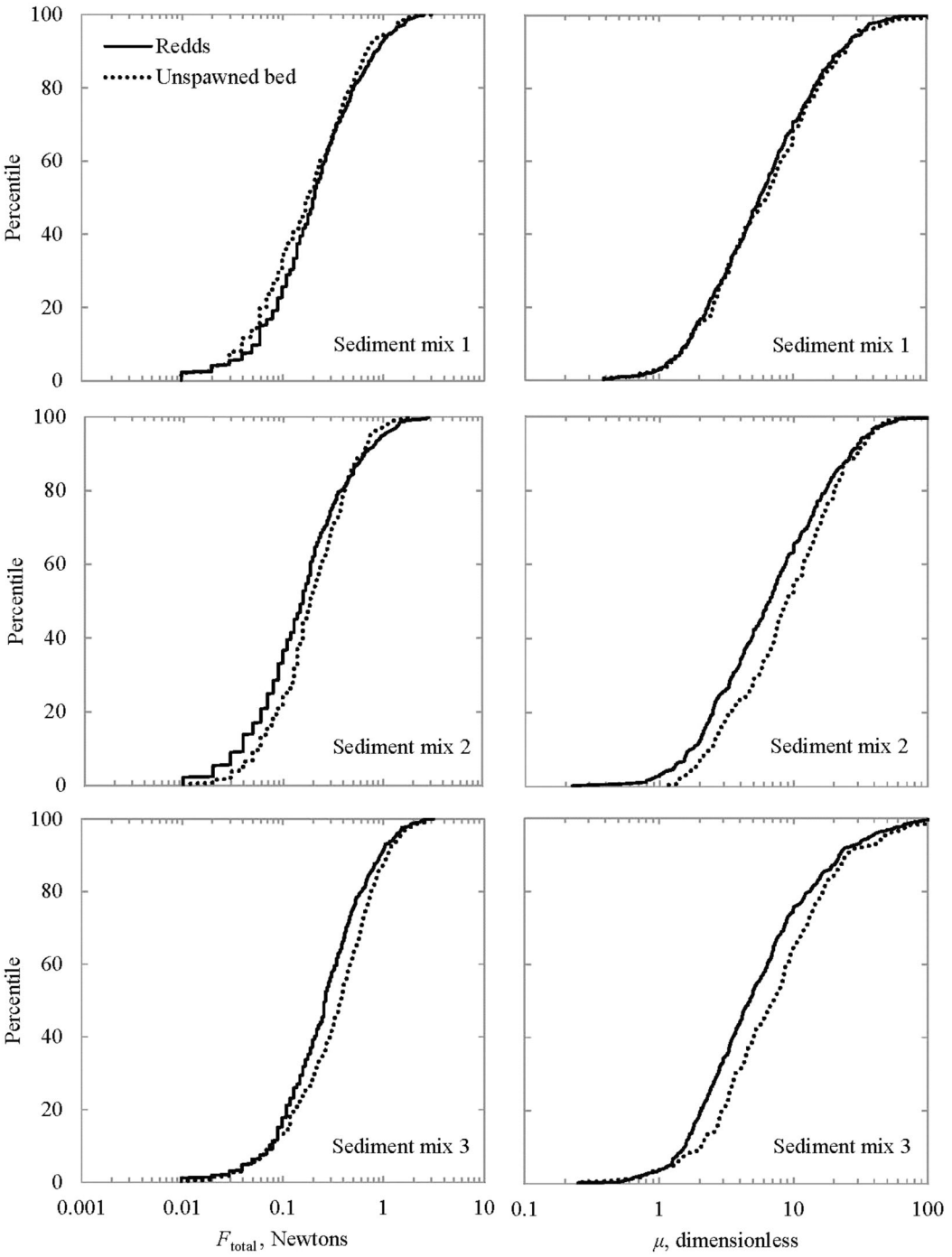

Figure 5. Cumulative distributions of (left column) the total force resisting grain movement (F_{total}) and (right column) friction coefficients (μ) for grain-size classes from −2 to −5 phi (4–32 mm) on redds and unspawned beds composed of sediment mix 1–3.

classes was 29% lower on the redd (15.3 Pa) than on the unspawned bed (21.5 Pa). As with local estimates of τ_b (section 3.2), observed differences in $\tau_{b_{avg}}$ are conservative because flow acceleration around the redd may have caused a lower entrainment threshold than would occur on unspawned areas located outside the influence of the redd.

Sediment transport on the redd caused downstream translation of the tailspill until it dispersed and scoured flush with the unspawned bed. Translation began in flows with $\tau_{b_{avg}} \leq 12.0$ Pa, when entrainment was limited to the crest and flanks of the tailspill slope. The mobile bed area expanded at 13.4 Pa to include

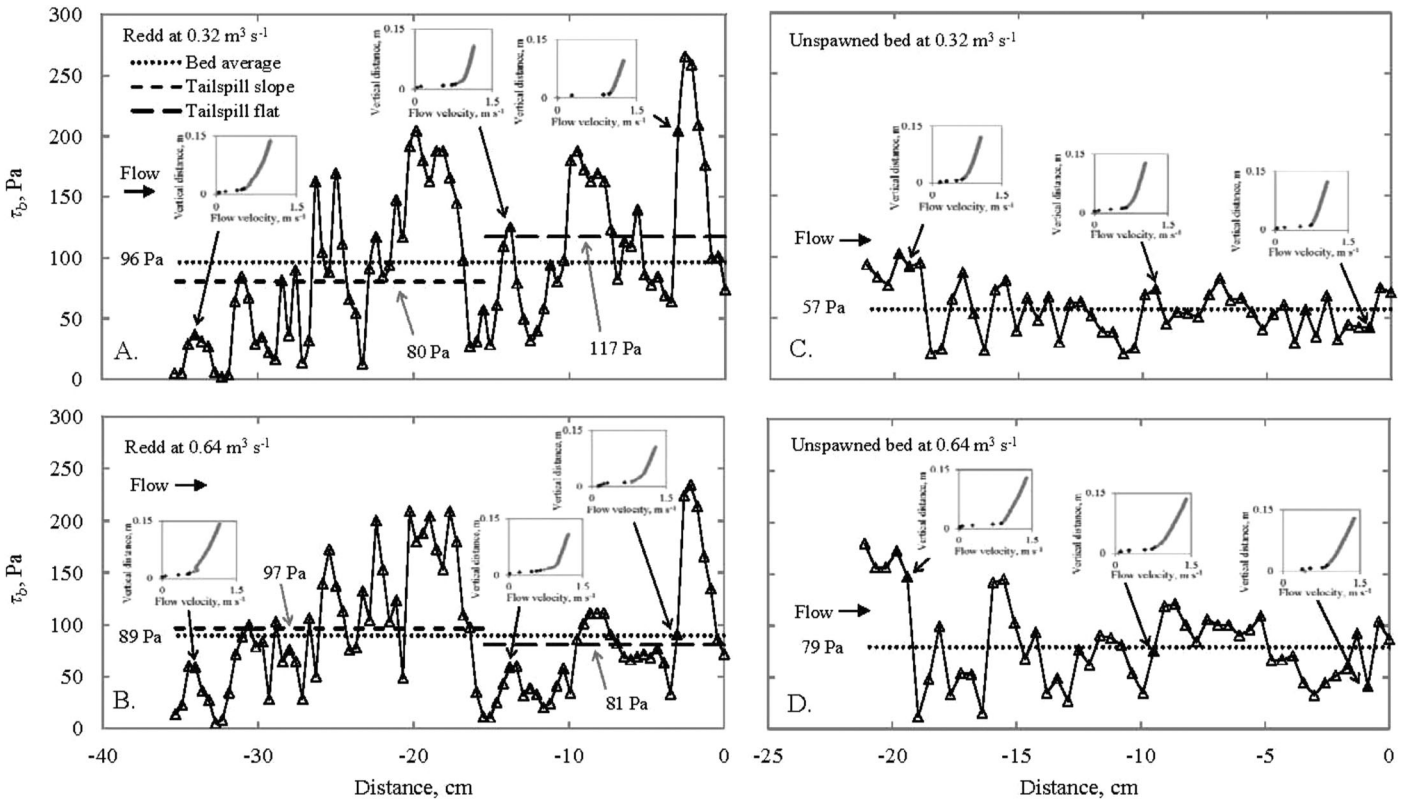

Figure 6. Boundary shear stress (τ_b; solid lines) estimated on (a, b) a redd and (c, d) unspawned bed surrounding the redd. Estimates of τ_b were made with the law of the wall using flow velocity profiles measured with particle image velocimetry at discharges of (top) 0.32 and (bottom) 0.64 m^3 s^{-1} in the flume. Inset figures are examples of the flow velocity profiles, with black points indicating the inner layer of the profiles that was used to estimate τ_b (section 2.7). Dotted lines indicate average values on both surfaces and dashed lines indicate average values on the tailspill slope and flat portions of the redd (Figure 1).

unspawned grains adjacent to the redd and grains on the tailspill flat. At this flow, mobile grains on the unspawned bed were transported downstream while mobile grains on the redd were mainly captured in the lee of the tailspill, promoting translation of the structure. Sustained mobility on the redd filled the lee area at around 14.9 Pa. Without a lee area to capture mobile sediment, the tailspill began to disburse as mobile grains transported downstream. As mobility continued, the tailspill lowered in elevation, which eroded grains from the lee area and accelerated dispersion of the tailspill. At 17.9 Pa, unspawned grains that were mobilized upstream of the redd deposited in and partially filled the pot. From 19.4 Pa through 20.4 Pa, entrainment on the unspawned bed expanded to include grains that were 16 to $<$24 mm in diameter while the redd tailspill rapidly eroded between 18.9 and 20.4 Pa. At 21.5 Pa, entrainment of grains $>$24 mm concluded mobility of unspawned size classes and completed filling the pot, which remained stable throughout the experiment. At a $\tau_{b_{avg}}$ of 23.0 Pa, the tailspill was eroded flush with the unspawned bed.

Mass transport rates of surface grains per unit area of spawned and unspawned portions of the bed support observations of redd translation followed by dispersal, and our conclusion that redds are unstable compared to unspawned beds (Figure 8). Although mass transport rates give the impression that the unspawned bed was initially more mobile, this is an artifact of the transient storage of grains mobilized on the redd. For instance, sediment entrained on the redd at 10.4 Pa was captured in the lee of the redd, which delayed transport of particles to the bed load traps until 14.9 Pa, when the lee filled and grains moved downstream into the traps (Figures 7 and 8). In contrast, the unspawned bed mobilized later than the redd (13.4 Pa, Figure 7), but these grains rapidly traversed the flume and were captured sooner by the bed load traps (14.0 Pa, Figure 8). We do not have an explanation for surface transport rates decreasing on both beds at 16.8 Pa, but they once again increased and nearly equalized between surfaces at 17.5 Pa (Figure 8). At 18.4 Pa, erosion of the tailspill promoted redd dispersion that sustained sediment transport rates in excess of those for the unspawned bed for the remainder of the experiment. This result and average mass transport rates being 4.5 times higher on the redd (0.38 g s^{-1} m^{-2}) than on the unspawned bed (0.08 g s^{-1} m^{-2}) confirm that redds were relatively unstable in our experiments.

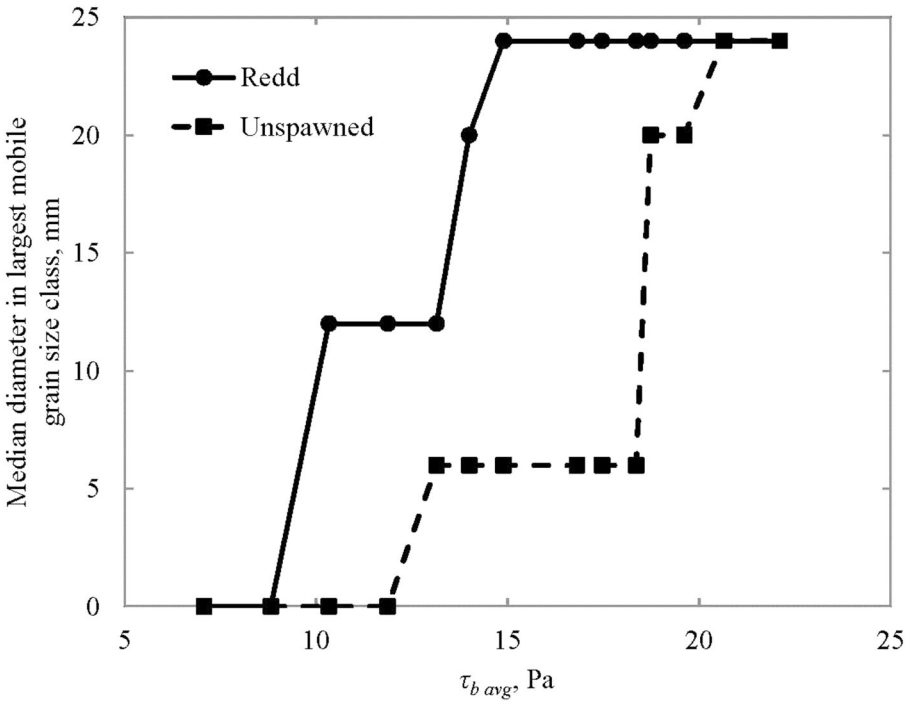

Figure 7. Visual measurements of grain mobility on a redd and surrounding unspawned bed plotted against the reach-average shear stress corrected for sidewall effects ($\tau_{b_{avg}}$; Appendix B).

4. Discussion

Our experiments demonstrate that redds are less stable than unspawned beds. This finding is supported by field observations of redd instability by *Lisle* [1989], *Rennie and Millar* [2000], and *Bigelow* [2003], but counters *Montgomery et al.*'s [1996] theoretical calculations that predicted redds are stable compared to unspawned beds. Our findings differed from those of *Montgomery et al*. [1996] because our study permitted observation of the destabilizing effects of spawning, which include bed loosening that decreases grain resistance to movement, and flow convergence over the redd that elevates boundary shear stress relative to that on planar unspawned beds. The combined outcome of these effects is that higher sediment transport rates occur where redds are constructed.

Our findings most directly apply to isolated redds that are unsheltered by flow obstructions and nearby redds, but *Montgomery et al*. [1996] also considered the effect of redd form drag on stability by treating redds as channel-spanning bed forms. Except perhaps in low-order channels, redds only occupy a portion of a channel's width. Therefore, in mid-order to high-order channels, it remains unclear whether form drag from redds extracts enough momentum to decrease boundary shear stress and protect downstream redds from erosion. Some insight into this question is provided by research involving dunes [*Engel*, 1981; *Nelson and Smith*, 1989], which suggests redds separated by streamwise distances greater than 4–6 times the amplitude of the upstream redd are unsheltered and may experience the relatively high boundary shear stress that we observed. However, redds built in spacings below this range might still experience elevated boundary shear stress from local variations in flow, including flow acceleration over and around redds and high turbulence generated by tailspill wakes. Turbulence effects may be suppressed when redds are irregularly spaced, as suggested by *Venditti*'s [2007] research that indicated form drag was 20% less on randomly spaced dunes than regular-spaced dunes. However, excavation of bar margins and smoothing of pool-riffle topography by high-density spawning [*Schuett-Hames*, 1996] can reduce channel roughness, potentially offsetting momentum losses from redd topography and leaving redds vulnerable to erosion. Overall, form drag from redds depends on the size and spacing of redd topography, with maximum form drag likely occurring at intermediate densities [e.g., *Yager et al*., 2007].

The size, shape, and orientation of redds also affect the stability of spawned beds. In general, the boundary shear stress on a redd varies with redd size relative to the flow width and depth. Larger redds experience

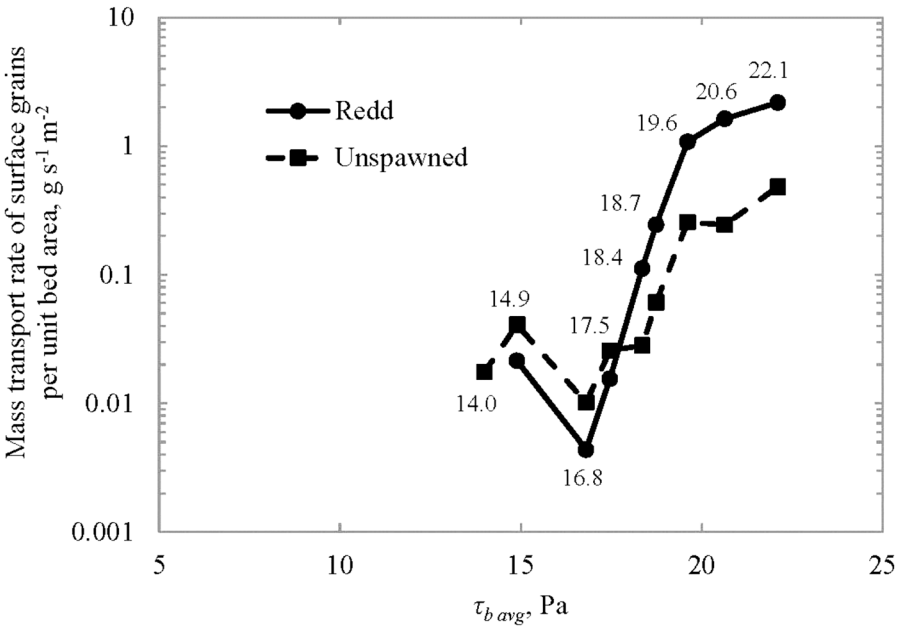

Figure 8. Mass transport rates of surface grains per unit area of the redd and surrounding unspawned bed in experiment 3 as a function of reach-average boundary shear stress corrected for sidewall effects ($\tau_{b_{avg}}$; Appendix B). Labels indicate specific $\tau_{b_{avg}}$ values.

greater flow convergence and boundary shear stress than planar beds, especially for shallower flows in smaller channels. Redds in teardrop shapes (used in this study and typical in nature) are streamlined and more stable than redds constructed in less streamlined shapes or with their long axis angled to flow. Variations from a streamlined form and flow-parallel alignment can therefore result in even lower redd stability than observed in our experiments. The teardrop shape and parallel alignment of redds results from flow dispersing grains during spawning and possibly also from probing behavior by the female salmon during construction of the redd [*Jones and Ball*, 1954]. Since probing behavior relies on a female's sense of flow, injury and environmental conditions may result in redds that are oddly shaped or angled to flow. We have observed injured (bear-bitten) female chum salmon building redds with the long axis obliquely angled to the primary flow direction. Turbidity can also lead to unusual redd shapes by disorienting the female and causing her to wander laterally while constructing the redd [*Lorenz and Eiler*, 1989]. In both these cases, constructed redds would likely exhibit lower stability than redds in the current study.

The inherent instability of redds suggests that embryos in the nest may be vulnerable to scour. However, field studies show that this may not be the case. *Rennie and Millar* [2000] found that scour of redd tailspills was greatest, while scour of egg pockets was no different from the adjacent unspawned bed. Greater scour of the tailspill is expected given the topographically forced increase in shear stress over the tailspill (section 3.2) and because elevated streamflow tends to smooth exogenous topography, such as redds [*Montgomery et al*., 1996]. Redd stratigraphy may have also influenced *Rennie and Millar*'s [2000] results. For example, our field excavations of redds and those made by others [*Hawke*, 1978; *Peterson and Quinn*, 1996] reveal a coarse surface layer, below which is a surface seal of fines, then a cover layer of unsorted sand and small gravel, followed by a bridge of medium gravel that overlies the egg pockets, which are composed of the largest grains in the area of redd construction (Figure 9). With this stratigraphy, tailspill scour should rapidly proceed after initial mobility since further erosion is only prevented by relatively small grains in the immediate subsurface. Once the tailspill erodes flush with the streambed, boundary shear stress will largely equalize between the redd and unspawned bed and reduce potential for differences in scour. At this point, coarse grains in egg pockets may offset loose packing in the redd and reduce or eliminate differences in scour between the redd and unspawned bed, as observed by *Rennie and Millar* [2000].

Redd mobility may increase the risk of fine sediment infiltration, which reduces survival of embryos in the nest. For example, strong negative relationships have been established between concentrations of fine sediment (typically $<$2 mm) in the streambed and embryo survival in laboratory and field studies [*Everest et al*., 1987;

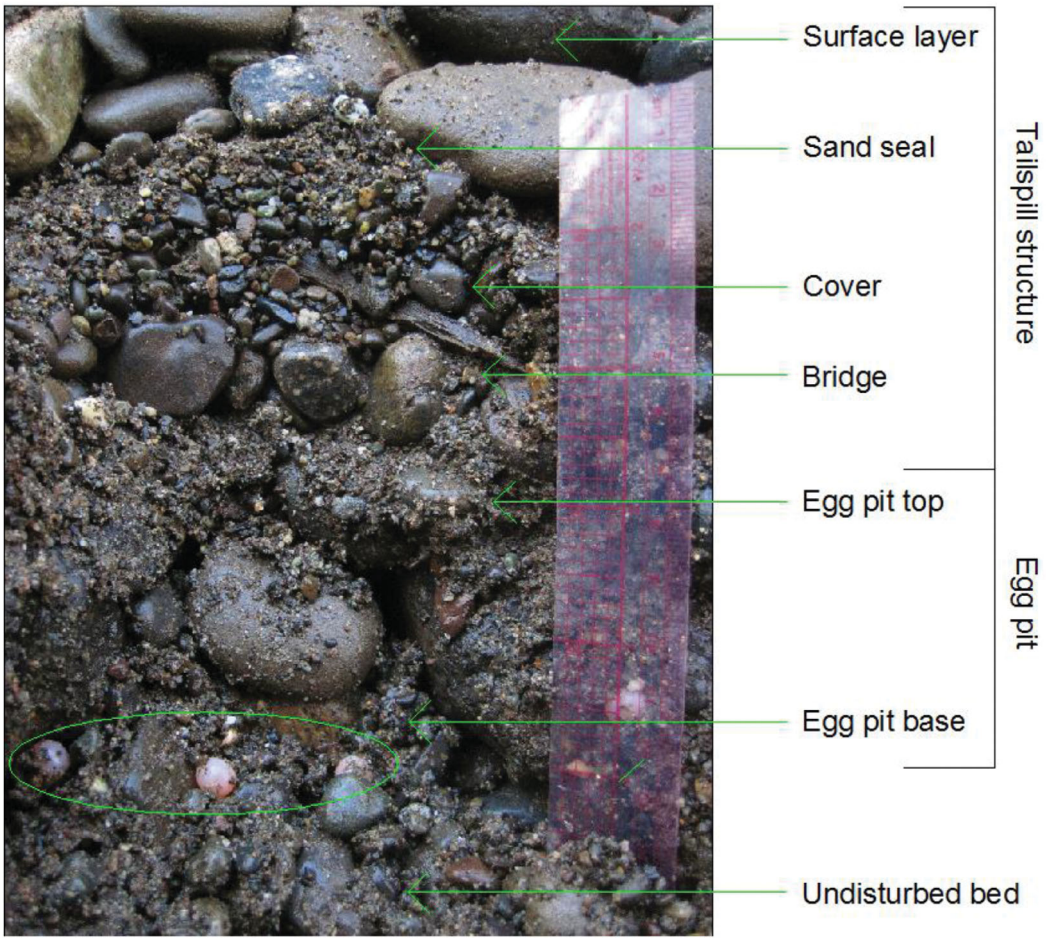

Figure 9. Stratigraphy of sediment in a dewatered chum salmon redd in Kennedy Creek. Eggs that rolled from the pit during excavation are circled.

Chapman, 1988]. Fines impact egg development and survival by reducing water flow to eggs [*Cordone and Kelly*, 1961], limiting alevin movement in gravel interstices [*Phillips et al.*, 1975], suffocating embryos by obstructing micropores in egg membranes [*Greig et al.*, 2005], or entombing embryos in the nest [*Koski*, 1966; *Vaux*, 1968; *May et al.*, 2009]. However, infiltration of fine sediment is often blocked by sand seals that form in the shallow subsurface of redds (Figure 9). Although bed mobility disrupts sand seals, they often reform after erosional events to help protect eggs from siltation [*Lisle*, 1989; *Meyer et al.*, 2005]. A potentially greater impact to embryo development than intrusion of fines may be tailspill erosion that reduces hyporheic flow through the redd, which is necessary for oxygenating eggs and flushing metabolic wastes [e.g., *Johnson*, 1980; *Tonina and Buffington*, 2009]. Gradients in hydraulic conductivity between the redd and unspawned bed may continue to generate hyporheic flow, but water flow to eggs in the nest will moreso depend on ambient pressure gradients (e.g., pool-riffle topography) following erosion of redd topography.

Our findings are based on a series of flume measurements that were conducted under limited experimental conditions. Results may have differed, for instance, if silt and clay-sized material had been included in the sediment mixtures. This would have generated relatively higher measurements of grain resistance (section 3.1) on unspawned beds due to sediment cohesion and mortaring [*Barzilai et al.*, 2013] that would have been disrupted by simulated spawning. Redds may have also exhibited somewhat higher stability in the mobility experiment (section 3.3) if they had been modeled after species of salmon that construct smaller structures (e.g., pink (*O. gorbuscha*) and sockeye (*O. nerka*) salmon), with correspondingly smaller redd topography for forcing flow convergence and increasing boundary shear stress [*DeVries*, 2012]. The opposite may have occurred, however, if redds had been modeled after Chinook salmon (*O. tshawytschta*) that construct larger redds than other species of Pacific salmon.

Our sediment transport results may also have differed if we had fed sediment to the flume during the experiment. With a sediment feed, the open structure of redd particles would be prone to fine sediment infiltration that could more tightly pack grains and reduce their mobility. However, a high sediment supply or a supply containing a large percentage of fines can cause textural fining that reduces bed-surface roughness and, in turn, increases near-bed velocities and bed load transport rates [*Dietrich et al*., 1989; *Wilcock*, 1998; *Wilcock and Crowe*, 2003]. Such effects would likely be moderated by spatial divergence of flow and bed load transport forced by the redd, perhaps focusing textural fining and higher transport rates where flow converges on the flanks of the redd. Granular transport can also extract momentum, altering boundary shear stress, channel competence, and bed load transport rates. Overall, the effects of sediment feed would depend on the volume and caliber of the supply, as well as the magnitude of the spatial divergence of flow and transport imposed by the redd, which is a function of redd size relative to flow depth and velocity. Our results control for such complexities, which limits them to cases of low sediment supply.

Another factor left unexamined in our experiments was the three-dimensional (3-D) interaction of flow with redds, as our velocity measurements were limited to a 2-D transect on the centerline of a redd. As a result, velocity measurements on the redd (section 3.2) did not account for lateral divergence of flow across the convex top of the redd or flow acceleration on the flanks of the redd that are expected to occur. Nor did we account for the pot depression, which is expected to shelter grains [*Hobbs*, 1937], recirculate flow [*Burner*, 1951], and lower boundary shear stress on this area of the redd, as in the trough of a dune. These expectations were supported by our visual observations, which showed that grain mobility first occurred on the flanks and crest of the tailspill, while grains in the pot remained in place for eventual burial by unspawned grains that were mobilized upstream of the redd (section 3.3). Even so, further investigation is warranted to characterize the 3-D flow structure on redds, adjacent unspawned beds, and unspawned beds at variable distances from redds. This information will lead to a better understanding of flow conditions that mobilize spawned surfaces and unspawned beds that are hydraulically influenced by redds.

Our finding that redds are structurally unstable leads to the suggestion that chronic reductions in spawning activity may decrease the amount of fine sediment that is entrained from the subsurface during mobility of loose, spawned beds. Diminution of this process and the flushing of fine sediment that occurs during redd building can lead to siltation of the intergravel environment and reduced incubation success [*Chapman*, 1988]. Such changes can negatively impact salmon populations and lead to decreased marine nutrients that spawners contribute to aquatic food webs [*Cedarholm et al*., 1999; *Wipfli and Baxter*, 2010] and riparian ecosystems [*Bilby et al*., 2003; *Drake and Naiman*, 2007], which, in turn, influence the growth and survival of juvenile salmon during their freshwater residency [*Scheuerell et al*., 2005].

5. Conclusions

Using a series of complementary experiments, our analyses show that redds are more mobile than unspawned bed surfaces. Evidence for this conclusion includes (1) distributions of entrainment forces were statistically similar or significantly lower for grains on redds than unspawned beds; (2) boundary shear stresses were up to 41% higher on a redd tailspill than the adjacent unspawned bed; (3) bed-average shear stress at observations of grain incipient motion was 22% lower on a redd than unspawned bed and 29% lower at the discharge that mobilized all grain-size classes on a redd; and (4) mass transport rates of surface grains were nearly 5 times higher on a redd than the surrounding unspawned bed. Greater mobility of redds may expose embryos in the nest to risk of scour, fine sediment infiltration, and reduced hyporheic flow. However, compensating effects may counter or reduce such risk (section 4). Our findings, combined with prior research indicating that mass spawning can mobilize about half the annual bed load yield [*Hassan et al*., 2008], suggest that chronically low salmon populations may lead to siltation of stream habitats and further declines in fish populations. Further quantifying this linkage may provide a defensible basis for managing salmon returns to promote streambed disturbances that may be required to sustain or restore salmon populations.

Appendix A: Scaling the Metal Spatula for Simulated Spawning

Redds were constructed in the flume with a metal spatula that was a scaled model of chum salmon caudal fins measured in Herman Creek near Haines, Alaska. Scaling the metal spatula was an important consideration because the size of redds and the caliber of sediment moved by spawners scales with fish size [*van den*

Berghe and Gross, 1984]. We preferred to scale the metal spatula from chum caudal fins in Kennedy Creek, but spawner carcasses were too degraded for these measurements. Instead, we used linear regression to relate paired measurements of the caudal fin width (W_f, mm) and fork length of female chum (F_L, mm; mid-eye to caudal fork) in Herman Creek: $W_f = 0.28(F_L) - 0.22$; $R^2 = 0.59$, $n = 13$. The regression equation was then used with the average fork length of female chum salmon measured in Kennedy Creek ($F_L = 602$ mm, $s = 39$ mm, $n = 27$) to estimate an average caudal fin width of 169 mm for Kennedy Creek chum. This value was scaled smaller by a factor of 3 (section 2.2) to set the width of the metal spatula (56 mm) for building redds in the flume.

Appendix B: Sidewall Correction

We determined the reach-average boundary shear stress on the bed ($\tau_{b_{avg}}$) by partitioning roughness between the flume walls and the granular bed using a modified version of the *Vanoni and Brooks* [1957] sidewall correction. In this analysis, the Darcy-Weisbach friction factor (f) and the Reynolds number (Re) are used with *Cheng*'s [2011] modification of the Colebrook-White equation to estimate friction from the hydrodynamically smooth walls of the flume (f_w)

$$f = \frac{8gRS}{\bar{u}^2} \tag{B1}$$

$$Re = \frac{4R\bar{u}}{\upsilon} \tag{B2}$$

$$\frac{1}{\sqrt{f_w}} = -2Log\left(2.51 \Big/ \frac{Re}{f}\sqrt{f_w^{1.5}}\right) \tag{B3}$$

where f is the total frictional resistance of the channel, g is gravitational acceleration, R is the hydraulic radius ($wh/(w + 2h)$, where w and h are the flume width and depth, respectively), S is the flume slope, $\bar{u}$ is the reach-average flow velocity, υ is kinematic viscosity, and f_w is solved iteratively. Values of f and f_w are used to isolate friction on the bed (f_b) following the *Vanoni and Brooks* [1957] method

$$f_b = f + \frac{2h}{w}(f - f_w) \tag{B4}$$

The partitioned bed-average shear stress on the granular bed is given by

$$\tau_{b_{avg}} = \rho g \frac{f_b}{f} RS \tag{B5}$$

where ρ is the density of water.

Acknowledgments
We thank Eric Beach of the Green Diamond Resource company for providing access to Kennedy Creek for this study. Laboratory and field assistance was provided by Cindy Buxton. The data used in this study are available upon request from the senior author. Research was supported by funding from the Cooperative State Research Service, U.S. Department of Agriculture, Project 2012-32100-06016 and a U.S. Geologic Survey 104B grant to the University of Idaho, Moscow. This publication is contribution 1082 of the Idaho Forest, Wildlife, and Range Experiment Station, College of Natural Resources, University of Idaho. We thank three anonymous reviewers for their input that improved this paper.

References

Adrian, R. J. (2005), Twenty years of particle image velocimetry, *Exp. Fluids*, *39*, 159–169.
Barzilai, R. J., B. Laronne, and I. Reid (2013), Effect of changes in fine-grained matrix on bedload sediment transport in a gravel-bed river, *Earth Surf. Processes Landforms*, *38*, 441–448.
Bigelow, P. E. (2003), Scour, fill, and salmon spawning in a northern California coastal stream, MS thesis, Dept. of Geol., Humboldt State Univ., Arcata, Calif.
Bilby, R. E., E. W. Beach, B. R. Fransen, J. K. Walter, and P. A. Bisson (2003), Transfer of nutrients from spawning salmon to riparian vegetation in Western Washington, *Trans. Am. Fish. Soc.*, *132*, 733–745.
Bjornn, T. C., and D. W. Reiser (1991), Habitat requirements of salmonids in streams, in *Influences of Forest and Rangeland Management on Salmonid Fishes and Their Habitat, Am. Fish. Soc. Spec. Pub. 19*, edited by W. R. Meehan, pp. 83–138, Am. Fish. Soc., Bethesda, Md.
Buffington, J. M., and D. R. Montgomery (1997), A systematic analysis of eight decades of incipient motion studies, with special reference to gravel-bedded rivers, *Water Resour. Res.*, *33*, 1993–2029.
Buffington, J. M., W. E. Dietrich, and J. W. Kirchner (1992), Friction angle measurements on a naturally formed gravel streambed: Implications for critical boundary shear stress, *Water Resour. Res.*, *28*, 411–425.
Burner, C. J. (1951), Characteristics of spawning nests of Columbia River salmon, in *Fishery Bulletin of the Fish and Wildlife Service, vol. 52, Fish. Bull. 61*, U.S. Gov. Print. Off., Washington, D. C.
Buxton, T. H., J. M. Buffington, D. Tonina, A. K. Fremier, and E. M. Yager (2015), Modeling the influence of salmon spawning on hyporheic exchange of marine-derived nutrients in gravel streambeds, *Can. J. Fish. Aquat. Sci.*, *72*, 1–13, doi:10.1139/cjfas-2014-0413.
Cedarholm, C. J., M. D. Kunze, T. Murota, and A. Sibatani (1999), Pacific salmon carcasses: Essential contributions of nutrients and energy for aquatic and terrestrial ecosystems, *Fisheries*, *24*, 6–15.
Chapman, D. W. (1988), Critical review of variables used to define effects of fines in redds of large salmonids, *Trans. Am. Fish. Soc.*, *117*, 1–21.

Cheng, N. S. (2011), Revisited Vanoni-Brooks sidewall correction, *Int. J. Sed. Res.*, *26*, 524–528.
Church, M. A., D. G. McLean, and J. F. Wolcott (1987), River bed gravels: Sampling and analysis, in *Sediment Transport in Gravel-Bed Rivers*, edited by C. R. Thorne, J. C. Bathurst, and R. D. Hey, pp. 43–88, John Wiley, N. Y.
Cordone, A. J., and D. W. Kelly (1961), The influence of fine sediment on the aquatic life of streams, *Calif. Fish Game*, *47*, 189–228.
DeVries, P. (1997), Riverine salmonid egg burial depths: Review of published data and implications for scour studies, *Can. J. Fish. Aquat. Sci.*, *54*, 1685–1698.
DeVries, P. (2012), Salmonid influences on rivers: A geomorphic fish tail, *Geomorphology*, *157*, 66–74.
Dietrich, W. E., J. W. Kirchner, H. Ideda, and F. Iseya (1989), Sediment supply and the development of the coarse surface layer in gravel bedded rivers, *Nature*, *340*, 215–217.
Drake, D. C., and R. J. Naiman (2007), Reconstruction of Pacific salmon abundance from riparian tree-ring growth, *Ecol. Appl.*, *17*, 1523–1542.
Engel, P. (1981), Length of flow separation over dunes, *J. Hydraul. Div. Am. Soc. Civ. Eng.*, *107*, 1133–1143.
Everest, F. H., R. L. Beschta, J. C. Scrivener, K. V. Koski, J. R. Sedell, and C. J. Cederholm (1987), Fine sediment and salmonid production—A paradox, in *Streamside Management and Forestry and Fishery Interactions, Contrib. 57*, edited by E. Salo and T. Cundy, pp. 98–142, Coll. of For. Resour., Univ. of Wash., Seattle, Wash.
Folk, R. L. (1974), *Petrology of Sedimentary Rocks*, Hemphill Publ. Co., Austin, Tex.
Francis, J. R. D. (1973), Experiments on the motion of solitary grains along the bed of a water-stream, *Proc. R. Soc. London, Ser. A.*, *332*, 443–471.
Gottesfeld, A. S., M. A. Hassan, J. F. Tunnicliffe, and R. W. Poirer (2004), Sediment dispersion in salmon spawning streams: The influence of floods and salmon redd construction, *J. Am. Water Resour. Assoc.*, *40*, 1071–1086.
Graham, D. J., S. P. Rice, and I. Reid (2005a), A transferable method for the automated sizing of river gravels, *Water Resour. Res.*, *41*, W07020, doi:10.1029/2004WR003868.
Graham, D. J., I. Reid, and S. P. Rice (2005b), Automated sizing of coarse-grained sediments: Image processing procedures, *Math. Geol.*, *37*, 1–28, doi:10.1007/s11004-005-8745-x.
Greig, S. M., D. A. Sear, and P. A. Carling (2005), The impact of fine sediment accumulation on the survival of incubating salmon progeny: Implications for sediment management, *Sci. Total Environ.*, *344*, 241–258.
Hassan, M. A., and M. Church (2000), Experiments on surface structure and partial sediment transport on a gravel bed, *Water Resour. Res.*, *36*, 1885–1895.
Hassan, M. A., et al. (2008), Salmon-driven bed load transport and bed morphology in mountain streams, *Geophys. Res. Lett.*, *35*, L04405, doi:10.1029/2007GL032997.
Hawke, S. P. (1978), Stranded redds of quinnat salmon in the Mathias River, South Island, New Zealand, *N. Z. J. Mar. Freshwater Res.*, *12*, 167–171.
Hobbs, D. F. (1937), Natural reproduction of quinnat salmon, brown and rainbow trout in certain New Zealand waters, *N. Z. Mar. Dep. Fish. Bull. 6*, 104 pp.
Isaak, D. J., R. F. Thurow, B. E. Rieman, and D. B. Dunham (2007), Chinook salmon use of spawning patches: Relative roles of habitat quality, size, and connectivity, *Ecol. Appl.*, *17*, 352–364.
Johnson, R. A. (1980), Oxygen transport in salmon spawning gravels, *Can. J. Fish. Aquat. Sci.*, *37*, 155–162.
Johnston, C. E., E. E. Andrews, and J. Pitlick (1998), In situ determination of particle friction angles of fluvial gravels, *Water Resour. Res.*, *34*, 2017–2030.
Jones, J. W., and J. H. Ball (1954), The spawning behavior of Brown trout and salmon, *Brit. J. Anim. Behav.*, *2*, 103–114.
Kellerhals, R., and D. I. Bray (1971), Sampling procedures for coarse fluvial sediments. *J. Hydraul. Div. Am. Soc. Civ. Eng.*, *97*, 1165–1180.
Keulegan, G. H. (1938), Laws of turbulent flow in open channels, *J. Res. Natl. Bur. Stand.*, *21*, 707–741.
Kondolf, G. M. (1988), Salmonid spawning gravels: A geomorphic perspective on their size distribution, modification by spawning fish, and criteria for gravel quality, PhD dissertation, Johns Hopkins Univ., Baltimore, Md.
Kondolf, G. M., and M. G. Wolman (1993), The sizes of salmonid spawning gravels, *Water Resour. Res.*, *29*, 2275–2285.
Koski, K. V. (1966), The survival of coho salmon (*Oncorhynchus kisutch*) from egg deposition to emergence in three Oregon coastal streams, MS thesis, Oreg. State Univ., Corvallis.
Lackey, R. T. (2000), Restoring wild salmon to the Pacific Northwest: Chasing an illusion? in *What We Don't Know About Pacific Northwest Fish Runs—An Inquiry Into Decision-Making*, edited by P. Koss and M. Katz, pp. 91–143, Portland State Univ., Portland, Oreg.
Lisle, T. E. (1989), Sediment transport and resulting deposition in spawning gravels, North Coastal California, *Water Resour. Res.*, 25, 1303–1319.
Lorenz, J. M., and J. H. Eiler (1989), Spawning habitat and redd characteristics of sockeye salmon in the glacial Taku River, British Columbia and Alaska, *Trans. Am. Fish. Soc.*, *118*, 495–502.
Madej, M. A. (1999), Temporal and spatial variability in thalweg profiles of a gravel bed river, *Earth Surf. Processes Landforms*, *24*, 1153–1169.
May, C. L., B. Pryor, T. E. Lisle, and M. Lang (2009), Coupling hydrodynamic modeling and empirical measures of bed mobility to predict the risk of scour and fill of salmon redds in a large regulated river, *Water Resour. Res.*, *45*, W05402, doi:10.1029/2007WR006498.
Meyer, C. B., M. D. Sparkman, and B. A. Klatte (2005), Sand seals in coho salmon redds: Do they improve egg survival?, *N. Am. J. Fish. Manage.*, *25*, 105–121.
Middleton, G. V., and J. B. Southard (1984), *Mechanics of Sediment Movement, Short Course 3*, 401 pp., Soc. of Econ. Paleontol. and Mineral., Providence, R. I.
Montgomery, D. R., J. M. Buffington, N. P. Peterson, D. Schuett-Hames, and T. P. Quinn (1996), Stream-bed scour, egg burial depths, and the influence of salmonid spawning on bed surface mobility and embryo survival, *Can. J. Fish. Aquat. Sci.*, *53*, 1061–1070.
Motamedi, A., H. Afzalimehr, V. Singh, and L. Dufresne (2014), Experimental study on the influence of dune dimensions on flow separation, *J. Hydrol. Eng.*, *19*, 78–86.
Nehlsen, W., J. E. Williams, and J. A. Lichatowich (1991), Pacific salmon at the crossroads, stocks at risk from California, Oregon, Idaho, and Washington, *Fisheries*, *16*, 4–21.
Nelson, J. M., and J. D. Smith (1989), Mechanics of flow over ripples and dunes, *J. Geophys. Res.*, *94*, 8146–8162.
Peterson, N. P., and T. P. Quinn (1996), Persistence of egg pocket architecture in redds of chum salmon, *Oncorhynchus keta*, *Environ. Biol. Fishes*, *46*, 243–253.
Phillips, R. W., R. L. Lantz, E. W. Claire, and J. W. Moring (1975), Some effects of gravel mixtures on emergence of coho salmon and steelhead trout fry, *Trans. Am. Fish. Soc.*, *104*, 461–466.
Rennie, C. D., and R. G. Millar (2000), Spatial variability of stream bed scour and fill: A comparison of scour depth in chum salmon (*Oncorhynchus keta*) redds and adjacent bed, *Can. J. Fish. Aquat. Sci.*, *57*, 928–938.

Scheuerell, M. D., P. S. Levin, R. W. Zabel, J. G. Williams, and B. L. Sanderson (2005), A new perspective on the importance of marine-derived nutrients to threatened stocks of Pacific salmon (*Oncorhynchus* spp.), *Can. J. Fish. Aquat. Sci.*, *62*, 961–964.
Schuett-Hames, D. E. (1996), Effects of scour and fill on salmonid incubation habitat in Kennedy Creek, a low-gradient alluvial channel in Mason and Thurston Counties, Washington, MS thesis, Evergreen State Coll., Olympia, Wash.
Smirnova, I. (1955), The effect of mechanical agitation at different periods of development on the eggs of autumn chum salmon [in Russian], *Dokl. Akad. Nauk SSSR*, *105*, 873–876. [Fish. Res. Board Can. Transl. Ser., Engl. Transl.,370].
Smith, A. K. (1973), Development and application of spawning velocity and depth criteria for Oregon salmonids, *Trans. Am. Fish. Soc.*, *102*, 312–316.
Stoesser, T., D. V. Terzi, W. Rodi, and N. R. B. Olsen (2006), Rans simulations and Les of flow over dunes at low relative submergence ratios, paper presented at 7th International Conference on Hydroscience and Engineering, Drexel Univ., Philadelphia, Pa.
Tonina, D., and J. M. Buffington (2009), A three-dimensional model for analyzing the effects of salmon redds on hyporheic exchange and egg pocket habitat, *Can. J. Fish. Aquat. Sci.*, *66*, 2157–2173.
van den Berghe, E. P., and M. R. Gross (1984), Female size and nest depth in coho salmon *(Oncorhynchus kisutch)*, *Can. J. Fish. Aquat. Sci.*, *41*, 204–206.
Vanoni, V. A., and N. H. Brooks (1957), Laboratory studies of the roughness and suspended load of alluvial streams, in *Sediment. Lab. Rep. E68*, 121 pp., Calif. Inst. Technol., Pasadena.
Vaux, W. G. (1968), Intergravel flow and interchange of water in a streambed, *Fish. Bull.*, *66*, 479–489.
Venditti, J. G. (2007), Turbulent flow and drag over fixed two- and three-dimensional dunes, *J. Geophys. Res.*, *112*, F04008, doi:10.1029/2006JF000650.
von Kármán, T. (1930), Mechanische Ähnlichkeit und Turbulenz, Nachrichten von der Gesellschaft der Wissenschaften zu Göttingen, Fachgruppe 1, *Mathematik*, *5*, 58–76.
Wilcock, P. R. (1998), Two-fraction model of initial sediment motion in gravel-bed rivers, *Science*, *280*, 410–412.
Wilcock, P. R., and J. C. Crowe (2003), Surface-based transport model for mixed-size sediment, *J. Hydraul. Eng.*, *129*, 120–128.
Wipfli, M. S., and C. V. Baxter (2010), Linking ecosystems, food webs, and fish production: Subsidies in salmonid watersheds, *Fisheries*, *35*, 373–387.
Wolman, M. G. (1954), A method of sampling coarse river-bed material, *Trans. AGU*, *35*, 951–966.
Yager, E. M., J. W. Kirchner, and W. E. Dietrich (2007), Calculating bed load transport in steep boulder bed channels, *Water Resour. Res.*, *43*, W07418, doi:10.1029/2006WR005432.